How to cite: *Angew. Chem. Int. Ed.* **2024**, *63*, e202403599
doi.org/10.1002/anie.202403599

VIP Supramolecular Polymers Very Important Paper

Dynamic Entwined Topology in Helical Covalent Polymers Dictated by Competing Supramolecular Interactions

*Lacey J. Wayment, Simon J. Teat, Shaofeng Huang, Hongxuan Chen, and Wei Zhang**

Abstract: Naturally occurring polymeric structures often consist of 1D polymer chains intricately folded and entwined through non-covalent bonds, adopting precise topologies crucial for their functionality. The exploration of crystalline 1D polymers through dynamic covalent chemistry (DCvC) and supramolecular interactions represents a novel approach for developing crystalline polymers. This study shows that sub-angstrom differences in the counter-ion size can lead to various helical covalent polymer (HCP) topologies, including a novel metal-coordination HCP (m-HCP) motif. Single-crystal X-ray diffraction (SCXRD) analysis of HCP–Na revealed that double helical pairs are formed by sodium ions coordinating to spiroborate linkages to form rectangular pores. The double helices are interpenetrated by the unreacted diols coordinating sodium ions. The reticulation of the m-HCP structure was demonstrated by the successful synthesis of HCP–K. Finally, ion-exchange studies were conducted to show the interconversion between HCP structures. This research illustrates how seemingly simple modifications, such as changes in counter-ion size, can significantly influence the polymer topology and determine which supramolecular interactions dominate the crystal lattice.

Natural polymeric structures, such as those found in DNA or collagen, typically incorporate both covalent and non-covalent bonds. The covalent bonds serve as the polymer's backbone, providing stability, while hydrogen bonding intertwines the polymer strands, forming helical structures.[1,2] There have been great strides in developing small molecule, oligomer, and polymeric helical structures.[1–5] Yet, it is rare to obtain single crystals that enable detailed analysis of the structure to clearly elucidate the structure-function properties.[6–8] Dynamic covalent chemistry (DCvC) has been utilized to design and synthesize crystalline polymers in a bottom-up approach using the principles of reticulation.[9–16] The dynamic nature of the bonds enables error correction as a thermodynamic control to favor the formation of structures that represent thermodynamic minimums. There is great interest in further understanding the factors that lead to certain structures being more thermodynamically favorable and the equilibrium between polymetric phases.[17–22] Additionally, it has been demonstrated that minor changes to the structure, such as larger counter-ions or the introduction of steric interactions, can change the interpenetration, stacking between layers, and topology.[23–27] Elucidating the crystal structures of the polymers through single-crystal XRD (SCXRD) or electron diffraction techniques enabled the detailed analysis of polymeric structures at the atomic level.[8,18,22,28–36] This provides a deeper understanding of the synergistic interplay between DCvC and supramolecular chemistry. Synthesizing samples suitable for these techniques is rare, and only a few comprise 1D polymer chains.[8,17,33,37–40]

The high conformational freedom of 1D polymers makes organizing the strands within 3D space challenging, so most 1D polymers are amorphous or semi-crystalline. Introducing weaker non-covalent interaction enables a thermodynamic driving force to further organize the polymer strands. The synergistic relationship between DCvC and supramolecular chemistry has yet to be broadly adopted due to the difficulty in predicting the structure. Thus far, metal-coordination, hydrogen bonding, and π- stacking have been used to construct both expected and unexpected architectures. However, little is known about the effect of multiple competing supramolecular interactions on the polymer topology. Previously, we reported the helical covalent polymer (HCP–Li) as a 1D polymer that adopts a double helical structure where the double helices are mechanically entwined by hydrogen bonding interactions of adjacent double helices.[8] The lithium counter-ions were observed inside the channels of the double helices without any coordinating interaction and were not part of the structure's backbone. Although this is an intriguing discovery, some important questions remain unanswered about the HCP polymers, such as will larger counter-ions adopt the same hydrogen bonding topology, participate in coordination with polymer strands, or demonstrate orthogonality with supramolecular chemistry? Additionally, small molecule double helices can exhibit a spring like motion when the counter-ion is exchanged.[41,42] This begs the question, can the HCPs exhibit dynamic modes of entwinement based on counter-ion exchange?

Herein, novel metal-coordinated helical covalent polymers (m-HCP) are reported. SCXRD unambiguously con-

[*] L. J. Wayment, S. Huang, H. Chen, Prof. W. Zhang
Department of Chemistry
University of Colorado Boulder
Boulder, CO-80309 (USA)
E-mail: wei.zhang@colorado.edu
Dr. S. J. Teat
Advanced Light Source, Lawrence Berkeley National Laboratory,
Department of Chemistry
University of California, Berkeley
Berkeley, CA-94720(USA)

firms the structure of HCP–Na, which shows the counterions are incorporated into the polymer's backbone by physically entwining double helices. The polymer strands adopt novel rectangular pores because the spiroborate linkages coordinate to the sodium ions, and the resulting helical structure forms two types of ion channels. Additionally, adjacent pairs are interpenetrated and held together through metal-coordination between the unreacted diols and the counter-ions. The crystal structure shows no strong hydrogen bonding interaction contributing to the organization of the 1D polymers. The reticulation of the m-HCP topology is established by demonstrating that HCP–K adopts the same topology. This also demonstrates a new mode of reticulation by incorporating the counter-ion into the backbone of the polymer. Furthermore, ion exchange experiments were used to investigate the dynamic nature of the different entwining modes and establish a novel pathway for synthesizing HCPs. The hydrogen bonded HCP structure can be converted to the m-HCPs. Interestingly, the m-HCPs cannot be converted back to the hydrogen bonded HCP under the same conditions.

HCP–Na synthesis involves reacting 2,3,6,7,10,11-hexahydroxytriphenylene (HHTP), trimethyl borate, and sodium hydroxide in 1.8 mL of a 1:1 aqueous acetonitrile/mesitylene mixture (Figure 1a). Single crystals of HCP–Na were obtained by stirring the reaction in a sealed ampule under vacuum at 80 °C for 12 hours. Subsequently, the reaction was heated at 120 °C for 30 days. The formation of HCP–Na follows an intermediate srs-phase, as previously reported (Figure S1).[20] Notably, the srs-phase persists more when using alternative solvent systems, such as 1:2 acetonitrile/mesitylene or boric acid as the boron source (Table S1). This persistence is attributed to the difference in the reaction kinetics and the availability of HHTP in solution. Previous work demonstrated that the spiroborate bond will not undergo metathesis with sodium as the counter-ion. So, HHTP or the unreacted diols likely trigger the bond exchange.[43] Adding additional water to facilitate the solvation of sodium hydroxide, increasing the ratio of non-polar solvents, or changing the initial boron species all affect the amount of HHTP present in the solution to participate in the exchange. The conditions screened for forming HCP–Na are summarized in Table S1.

The HCP–Na single crystals exhibit a rectangular bipyramid shape, as revealed by SEM and optical microscope analyses, with an average length ranging from 20 to 30 μm (Figure 1b). The largest crystals reach up to 50 μm (Figure 1b). The FT-IR spectrum of HCP–Na shows the

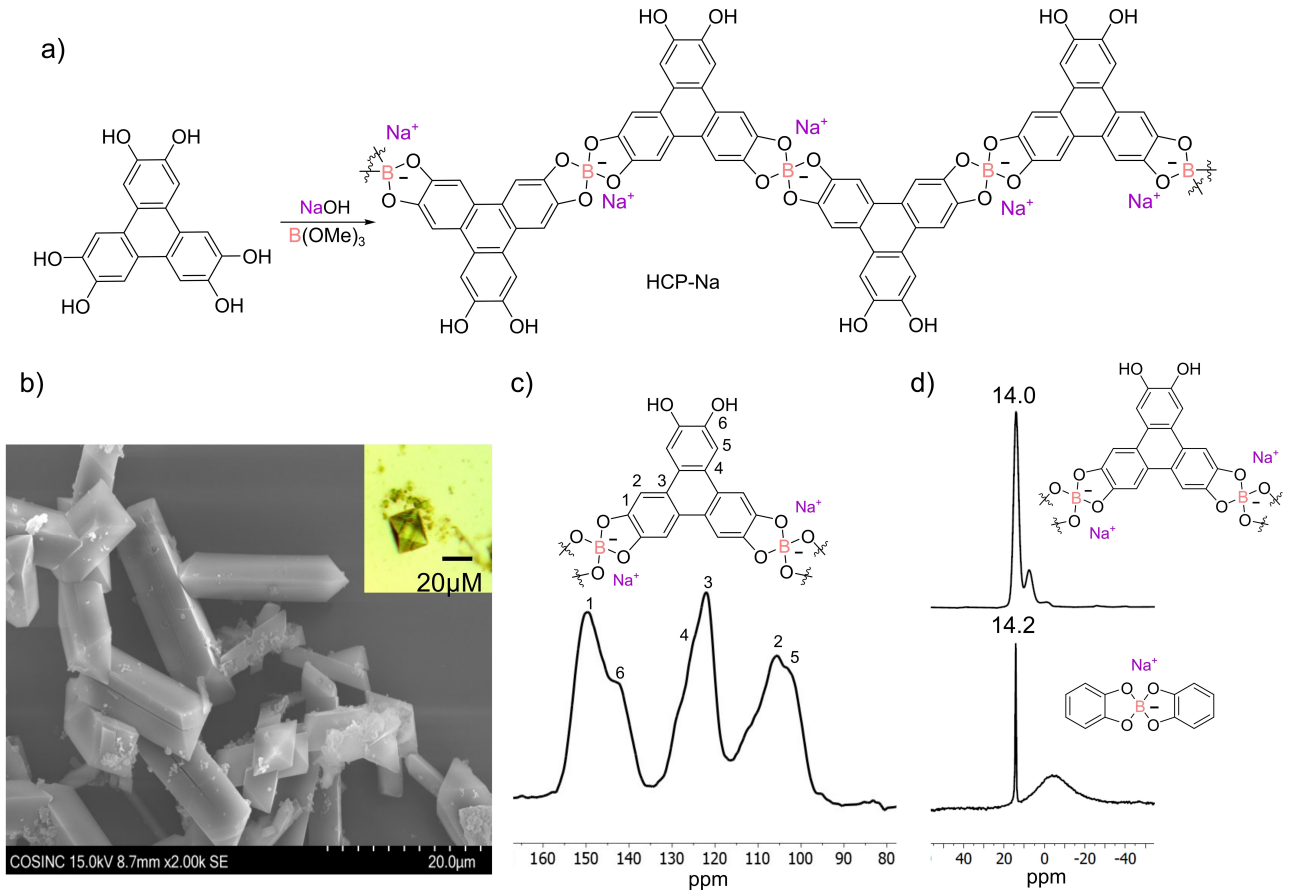

Figure 1. Synthesis and chemical characterization of HCP–Na. (a) Synthetic scheme of HCP–Na. (b) SEM of average-sized single crystals from HCP–Na. Insert: Optical image of the largest single crystals that were observed. (c) Solid-state ^{13}C spectrum of HCP–Na. The non-equivalent aryl carbon atoms are labeled 1–6. (d) The solid-state ^{11}B spectrum of HCP–Na and compound **1**.

presence of the B–O stretch at 1043 cm^{-1} and a reduction in the intensity of the hydroxyl peak (Figure S2). The solid-state carbon NMR spectrum displays signal splitting, attributed to the dissymmetry of the monomer due to the unreacted diols (Figure 1c). The solid-state boron NMR spectrum reveals a prominent signal at 14.0 ppm, aligning well with compound **1** (Figure 1d) and consistent with previous literature reports.[8,44]

The structure of HCP–Na was elucidated by SCXRD using a synchrotron light source with a discrepancy factor R of 7.36 %, which enables a detailed evaluation of the structure. The unit cell of HCP–Na is orthorhombic with a space group of I222 and dimensions of $a = 15.2478$ Å, $b = 17.8361$ Å, and $c = 17.8380$ Å. The HHTP and spiroborate linkages form helical 1D polymers entwined by sodium ions. Every other spiroborate along the 1D strands are linked through a sodium ion and extends the helical pitch of the 1D polymer strands to 31.61 Å (Figure 2a). The double helices adopt rectangular pores to accommodate the bridging sodium ions inside the channels. The rectangular pore dimensions are 10.62 Å by 6.18 Å, and the spiroborate groups display alternating dihedral angles of 67° and 73° (Figure 2b). Adjacent double helices are inserted into and held together by coordinating the sodium ions (Figure 2c and d). The rectangular pores also enable the formation of two unique channels, highlighted as purple and blue in Figure 2c. The channel adjacent to the double helices (blue) shows coordination of sodium ions and displays some disorder. In contrast, there is little disorder of the sodium ion in the double helix channel (purple). Adjacent polymer strands are interpenetrated and held together through the coordination of the sodium ion through unreacted diols (Figure 2d). The crystal structure contained no evidence of any strong hydrogen bonding interactions with the unreacted diols. There was uncertainty in the position of the hydrogen on the unreacted diol, which suggests that they don't strongly contribute to the overall structure as previously observed.[8] The minimal distance between the oxygen of the spiroborate and unreacted diol spans 2.94 Å. If the hydrogen bond angle was 180° then the hydrogen bonding interaction would be moderate to weak. This change is due to the distortion of the polymer strands to accommodate the coordination of the sodium ions.

Theoretically, the ion channels of the hydrogen bonded HCP are large enough to accommodate the sodium and potassium ions without metal coordination. Thus, the phase purity of the bulk HCP–Na was evaluated by comparing the bulk experimental PXRD pattern to the simulated diffraction pattern (Figure 3a). A simulation of the HCP–Na PXRD pattern was created from the single crystal data and matches well with the experimental pattern. There are some differences in the signal intensities that can be attributed to the difference in temperature during collection or some disorder of solvent molecules within the channels rather than mixed phases. Next, reticulation of this new mode of entwinement was evaluated by switching the counter-cations from sodium ions to potassium ions.

We posited that the alteration in the entwinement mode between the strands (HCP–Li vs. HCP–Na) was influenced by the larger counter-ion size. The m-HCP topology adds significance since it offers a secondary method of reticulation, distinct from merely modifying the organic building blocks, as the counter-ion is incorporated into the backbone of the structure. To assess the reticulation of this new entwinement mode, potassium ions were employed. HCP–K can be synthesized by utilizing similar methods, such as directly or utilizing phenol as a modulator (Figure 3b). SEM analysis showed that the crystals are not a single domain as indicated by uneven surface (Figure S4). FT-IR also confirms the formation of the spiroborate linkage with the

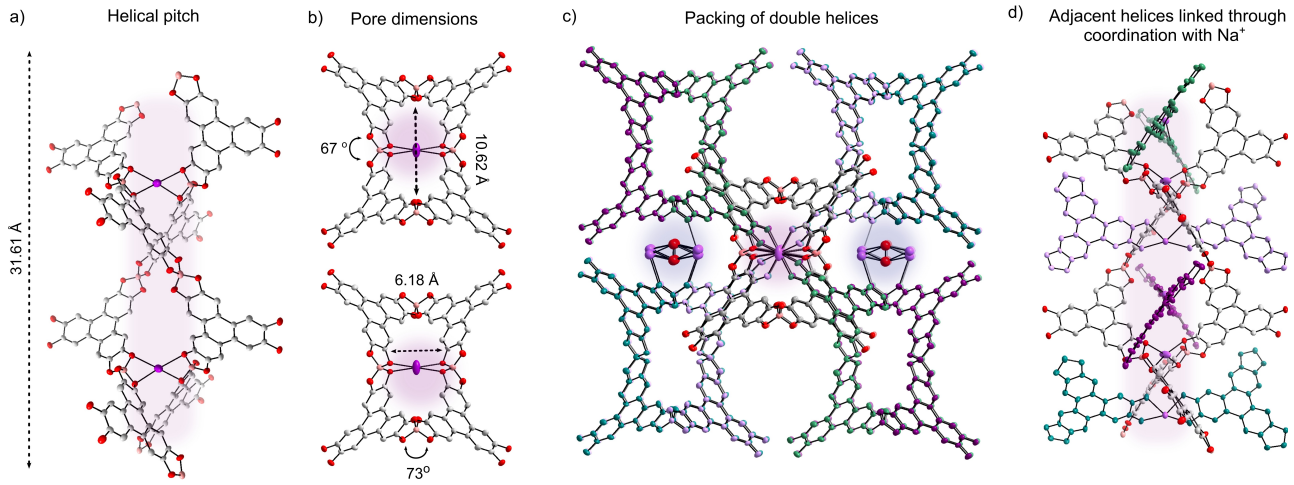

Figure 2. Single-crystal structure of HCP–Na. The physical dimensions of HCP–Na helices are where the channels are highlighted in purple and blue to indicate if they are within the double helices or adjacent, respectively. (a) The helical pitch of entwined 1D polymer strands with coordinated sodium ions. (b) Top-down view of the rectangular pores of the double helices where the pore dimension is 6.18 Å by 10.62 Å when measuring boron to boron. Top-down view (c) and side view (d) of the double helices packed together. A second sodium ion channel exists between adjacent helices. There is some disorder in the position of the ion. (d) The adjacent double helices pairs are linked through the unreacted diols coordinating sodium ions. Solvent molecules are removed for better clarity of the structure.

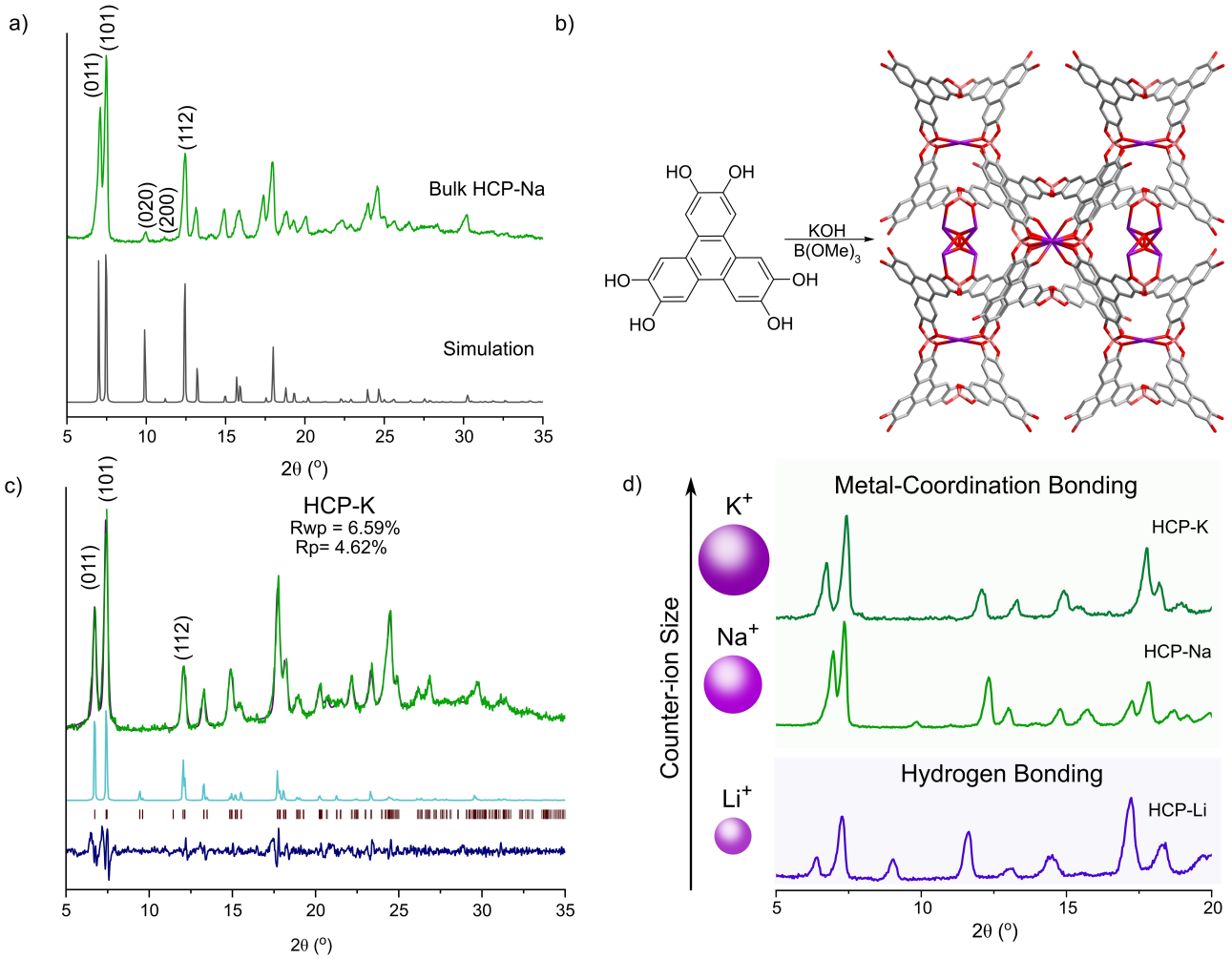

Figure 3. Bulk synthesis of HCP–Na and HCP–K. (a) Bulk HCP–Na compared to the simulation where the first five miller planes are identified. (b) the synthesis of HCP–K that forms the m-HCP topology. (c) Pawly refinement of HCP–K. Green is the experiment data; black is the refined pattern; light blue is the simulation; purple dashed represents the miller plane locations; and dark blue is the difference between the experimental and theoretical diffraction patterns. (d) A comparison of the diffraction patterns of HCP–Li, HCP–Na, and HCP–K. HCP–Li adopts a hydrogen-bonded HCP structure, while HCP–Na and HCP–K adopts the new m-HCP topology.

appearance of the B–O stretch at 1036 cm^{-1} and a reduction of the hydroxyl peak (Figure S3). The solid-state carbon NMR shows splitting of the aryl carbon signals due to the unreacted diols (Figure S5). Solid state boron NMR shows the spiroborate signal at 13.9 ppm and matches well with compound **2** (Figure S6).

The experimental diffraction pattern of HCP–K matches well with the new m-HCP topology. A model was built based on the HCP–Na crystal structure in Materials Studio. The solvent was removed to simplify the model, and the second ion channel was retained in the model. The unit cell dimensions were found to be $a = 15.4737$ Å, $b = 18.4251$ Å, and $c = 18.7580$ Å with a space group of I222 through Pawley refinement (RWP = 6.59 % and RP = 4.62 %) (Figure 3c). By comparing the crystal structures and the PXRD patterns, there is a contraction in the unit cell size when the m-HCP topology is adopted compared to the hydrogen bonding topology, particularly in the b and c dimensions of the unit cell. When the counter-ion is changed from sodium to potassium, then the unit cell is expanded in the b and c dimensions while there is a slight contraction in the a dimension. Sodium and potassium ions generally require more coordinating groups. Likely, metal-coordination becomes more favorable when the counter-ion becomes larger due an increase in electrostatic attraction as the distance between larger counter-ions and spiroborate groups decreases.

This expansion and contraction of the crystal structure can be envisioned to mimic a spring structure. To evaluate the HCPs in this capacity, they were subjected to ion exchange studies to test crystal to crystal transformation (Figure 4). The flexibility of the spiroborate linkages and the demonstrated ion conductivity of HCP-Li[45] enables the transformation of HCP to the new m-HCPs. An isolated polycrystalline sample of HCP–Li was treated with 1 eq of sodium tert-butoxide in acetonitrile. PXRD showed the conversion of HCP–Li to HCP–Na within 24 hours (Figure S7). When the sample was treated with 1 eq of lithium

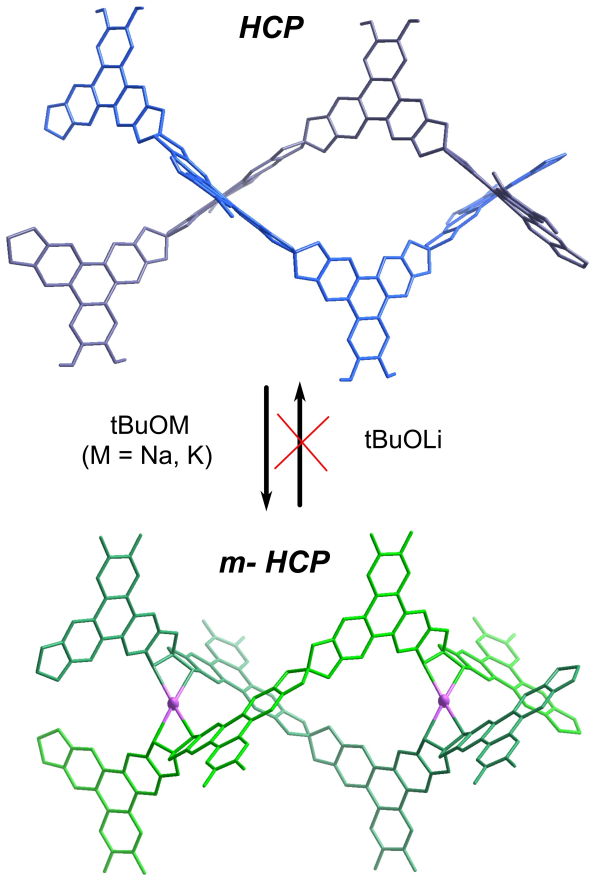

Figure 4. Scheme of ion-exchange studies. HCP samples were suspended in *tert*-butoxide salts dissolved in acetonitrile and left to exchange at room temperature.

tert-butoxide in acetonitrile there was no conversion back to HCP–Li after 24 h, and the sample showed a degradation in crystallinity after the second treatment (Figure S7). HCP–K can also be formed though ion exchange when HCP–Li is treated with potassium tert-butoxide (Figure S8). These ion exchange studies show that the HCP structures can be interconverted and considered an alternative method to synthesize new HCPs.

In conclusion, this work introduces a novel m-HCP topology that provides a unique approach to tuning HCP topologies through variations in counter-ion size and competing supramolecular interactions. A comprehensive single crystal analysis of HCP–Na offers a detailed insight into the m-HCP topology. The synthesis of HCP–K establishes the reticulation of m-HCP. This topology incorporates the counter-ion into the backbone of the polymeric structure. Thus, offering a novel alternative method to tune the dimensions of the crystal structure. Ion-exchange studies enable interconversion of HCP structures and unveil an alternative synthetic pathway for constructing HCP structures. This research significantly contributes to a deeper understanding of the interplay between DCvC and supramolecular chemistry, paving the way for the precise design of materials at the atomic level. As this field expands, polymers with more sophisticated structure motifs will become synthetically attenable for advanced functionality.

Supporting Information

The authors have cited additional references within the Supporting Information.[46–52]

Acknowledgements

W. Z. thanks the support from the National Science Foundation (CHE-2108197). This research used resources from the Advanced Light Source, which is a DOE Office of Science User Facility under contract no. DE-AC02-05CH11231.

Conflict of Interest

The authors declare no conflict of interest.

Data Availability Statement

The data that support the findings of this study are available in the supplementary material of this article.

Keywords: Dynamic Covalent Chemistry · Helical Covalent Polymers · Structure Elucidation · Supramolecular Chemistry · Spiroborates

[1] E. Yashima, K. Maeda, H. Iida, Y. Furusho, K. Nagai, *Chem. Rev.* **2009**, *109*, 6102–6211.
[2] T. Nakano, Y. Okamoto, *Chem. Rev.* **2001**, *101*, 4013–4038.
[3] D. J. Hill, M. J. Mio, R. B. Prince, T. S. Hughes, J. S. Moore, *Chem. Rev.* **2001**, *101*, 3893–4012.
[4] D.-W. Zhang, X. Zhao, J.-L. Hou, Z.-T. Li, *Chem. Rev.* **2012**, *112*, 5271–5316.
[5] E. Yashima, N. Ousaka, D. Taura, K. Shimomura, T. Ikai, K. Maeda, *Chem. Rev.* **2016**, *116*, 13752–13990.
[6] H. Kusanagi, Y. Chatani, H. Tadokoro, *Polymer* **1994**, *35*, 2028–2039.
[7] Y. Wang, Y. He, Z. Yu, J. Gao, S. ten Brinck, C. Slebodnick, G. B. Fahs, C. J. Zanelotti, M. Hegde, R. B. Moore, B. Ensing, T. J. Dingemans, R. Qiao, L. A. Madsen, *Nat. Commun.* **2019**, *10*, 801.
[8] Y. Hu, S. J. Teat, W. Gong, Z. Zhou, Y. Jin, H. Chen, J. Wu, Y. Cui, T. Jiang, X. Cheng, W. Zhang, *Nat. Chem.* **2021**, *13*, 660–665.
[9] A. P. Côté, A. I. Benin, N. W. Ockwig, M. O'Keeffe, A. J. Matzger, O. M. Yaghi, *Science* **2005**, *310*, 1166–1170.
[10] M. O'Keeffe, M. A. Peskov, S. J. Ramsden, O. M. Yaghi, *Acc. Chem. Res.* **2008**, *41*, 1782–1789.
[11] Y. Jin, Q. Wang, P. Taynton, W. Zhang, *Acc. Chem. Res.* **2014**, *47*, 1575–1586.
[12] Y. Jin, Y. Hu, W. Zhang, *Nat. Chem. Rev.* **2017**, *1*, 0056.
[13] L. J. Wayment, Z. Lei, Y. Jin, W. Zhang, *CCS Chem.* **2023**, *5*, 2194–2206.

[14] S. Kandambeth, K. Dey, R. Banerjee, *J. Am. Chem. Soc.* **2019**, *141*, 1807–1822.
[15] K. Geng, T. He, R. Liu, S. Dalapati, K. T. Tan, Z. Li, S. Tao, Y. Gong, Q. Jiang, D. Jiang, *Chem. Rev.* **2020**, *120*, 8814–8933.
[16] A. M. Evans, M. J. Strauss, A. R. Corcos, Z. Hirani, W. Ji, L. S. Hamachi, X. Aguilar-Enriquez, A. D. Chavez, B. J. Smith, W. R. Dichtel, *Chem. Rev.* **2022**, *122*, 442–564.
[17] T. Ma, J. Li, J. Niu, L. Zhang, A. S. Etman, C. Lin, D. Shi, P. Chen, L.-H. Li, X. Du, J. Sun, W. Wang, *J. Am. Chem. Soc.* **2018**, *140*, 6763–6766.
[18] C. Gropp, T. Ma, N. Hanikel, O. M. Yaghi, *Science* **2020**, *370*, eabd6406.
[19] Y. Liu, J. Li, J. Lv, Z. Wang, J. Suo, J. Ren, J. Liu, D. Liu, Y. Wang, V. Valtchev, S. Qiu, D. Zhang, Q. Fang, *J. Am. Chem. Soc.* **2023**, *145*, 9679–9685.
[20] L. J. Wayment, X. Wang, S. Huang, M. S. McCoy, H. Chen, Y. Hu, Y. Jin, S. Sharma, W. Zhang, *J. Am. Chem. Soc.* **2023**, *145*, 15547–15552.
[21] B. Gui, J. Xin, Y. Cheng, Y. Zhang, G. Lin, P. Chen, J.-X. Ma, X. Zhou, J. Sun, C. Wang, *J. Am. Chem. Soc.* **2023**, *145*, 11276–11281.
[22] X. Wang, Y. Wada, T. Shimada, A. Kosaka, K. Adachi, D. Hashizume, K. Yazawa, H. Uekusa, Y. Shoji, T. Fukushima, M. Kawano, Y. Murakami, *J. Am. Chem. Soc.* **2024**, *146*, 1832–1838.
[23] Y. Liu, Y. Ma, J. Yang, C. S. Diercks, N. Tamura, F. Jin, O. M. Yaghi, *J. Am. Chem. Soc.* **2018**, *140*, 16015–16019.
[24] Y. Xie, J. Li, C. Lin, B. Gui, C. Ji, D. Yuan, J. Sun, C. Wang, *J. Am. Chem. Soc.* **2021**, *143*, 7279–7284.
[25] X. Wu, X. Han, Y. Liu, Y. Liu, Y. Cui, *J. Am. Chem. Soc.* **2018**, *140*, 16124–16133.
[26] Y. Wang, Y. Liu, H. Li, X. Guan, M. Xue, Y. Yan, V. Valtchev, S. Qiu, Q. Fang, *J. Am. Chem. Soc.* **2020**, *142*, 3736–3741.
[27] Y. Xiao, Y. Ling, K. Wang, S. Ren, Y. Ma, L. Li, *J. Am. Chem. Soc.* **2023**, *145*, 13537–13541.
[28] T. Ma, E. A. Kapustin, S. X. Yin, L. Liang, Z. Zhou, J. Niu, L.-H. Li, Y. Wang, J. Su, J. Li, X. Wang, W. D. Wang, W. Wang, J. Sun, O. M. Yaghi, *Science* **2018**, *361*, 48–52.
[29] D. Beaudoin, T. Maris, J. D. Wuest, *Nat. Chem.* **2013**, *5*, 830–834.
[30] Z. Zhou, L. Zhang, Y. Yang, I. J. Vitorica-Yrezabal, H. Wang, F. Tan, L. Gong, Y. Li, P. Chen, X. Dong, Z. Liang, J. Yang, C. Wang, Y. Hong, Y. Qiu, A. Gölzhäuser, X. Chen, H. Qi, S. Yang, W. Liu, J. Sun, Z. Zheng, *Nat. Chem.* **2023**, *15*, 841–847.
[31] B. Yu, R.-B. Lin, G. Xu, Z.-H. Fu, H. Wu, W. Zhou, S. Lu, Q.-W. Li, Y. Jin, J.-H. Li, Z. Zhang, H. Wang, Z. Yan, X. Liu, K. Wang, B. Chen, J. Jiang, *Nat. Chem.* **2024**, *16*, 114–121.
[32] B. Yu, W. Li, X. Wang, J.-H. Li, R.-B. Lin, H. Wang, X. Ding, Y. Jin, X. Yang, H. Wu, W. Zhou, J. Zhang, J. Jiang, *J. Am. Chem. Soc.* **2023**, *145*, 25332–25340.
[33] H.-S. Xu, Y. Luo, X. Li, P. Z. See, Z. Chen, T. Ma, L. Liang, K. Leng, I. Abdelwahab, L. Wang, R. Li, X. Shi, Y. Zhou, X. F. Lu, X. Zhao, C. Liu, J. Sun, K. P. Loh, *Nat. Commun.* **2020**, *11*, 1434.
[34] A. M. Evans, L. R. Parent, N. C. Flanders, R. P. Bisbey, E. Vitaku, M. S. Kirschner, R. D. Schaller, L. X. Chen, N. C. Gianneschi, W. R. Dichtel, *Science* **2018**, *361*, 52–57.
[35] J. Li, C. Lin, T. Ma, J. Sun, *Nat. Commun.* **2022**, *13*, 4016.
[36] T. Sun, W. Lei, Y. Ma, Y.-B. Zhang, *Chin. J. Chem.* **2020**, *38*, 1153–1166.
[37] Y. Liu, Y. Ma, Y. Zhao, X. Sun, F. Gándara, H. Furukawa, Z. Liu, H. Zhu, C. Zhu, K. Suenaga, P. Oleynikov, A. S. Alshammari, X. Zhang, O. Terasaki, O. M. Yaghi, *Science* **2016**, *351*, 365–369.
[38] E. De Bolòs, M. Martínez-Abadía, F. Hernández-Culebras, A. Haymaker, K. Swain, K. Strutyński, B. L. Weare, J. Castells-Gil, N. M. Padial, C. Martí-Gastaldo, A. N. Khlobystov, A. Saeki, M. Melle-Franco, B. L. Nannenga, A. Mateo-Alonso, *J. Am. Chem. Soc.* **2022**, *144*, 15443–15450.
[39] B.-T. Liu, S.-H. Gong, X.-T. Jiang, Y. Zhang, R. Wang, Z. Chen, S. Zhang, K. O. Kirlikovali, T.-F. Liu, O. K. Farha, R. Cao, *Nat. Synth.* **2023**, *2*, 873–879.
[40] Y. Yang, E. Lin, S. Wang, T. Wang, Z. Wang, Z. Zhang, *J. Am. Chem. Soc.* **2024**, *146*, 782–790.
[41] N. Ousaka, K. Shimizu, Y. Suzuki, T. Iwata, M. Itakura, D. Taura, H. Iida, Y. Furusho, T. Mori, E. Yashima, *J. Am. Chem. Soc.* **2018**, *140*, 17027–17039.
[42] K. Miwa, Y. Furusho, E. Yashima, *Nat. Chem.* **2010**, *2*, 444–449.
[43] H. Chen, Y. Hu, C. Luo, Z. Lei, S. Huang, J. Wu, Y. Jin, K. Yu, W. Zhang, *J. Am. Chem. Soc.* **2023**, *145*, 9112–9117.
[44] X. Wang, M. Bahri, Z. Fu, M. A. Little, L. Liu, H. Niu, N. D. Browning, S. Y. Chong, L. Chen, J. W. Ward, A. I. Cooper, *J. Am. Chem. Soc.* **2021**, *143*, 15011–15016.
[45] Y. Hu, N. Dunlap, H. Long, H. Chen, L. J. Wayment, M. Ortiz, Y. Jin, A. Nijamudheen, J. L. Mendoza-Cortes, S.-H. Lee, W. Zhang, *CCS Chem.* **2021**, *3*, 2762–2770.
[46] F. C. Krebs, N. C. Schiødt, W. Batsberg, K. Bechgaard, *Synthesis* **1997**, 1285–1290.
[47] A. Bruker, APEX3 Package, APEX3, SAINT and SADABS. **2016**.
[48] L. Palatinus, G. Chapuis, *J. Appl. Crystallogr.* **2007**, *40*, 786–790.
[49] L. Palatinus, S. J. Prathapa, S. V. Smaalen, *J. Appl. Crystallogr.* **2012**, *45*, 575–580.
[50] L. J. Farrugia, *J. Appl. Crystallogr.* **1999**, *32*, 837–838.
[51] G. M. Sheldrick, *Acta Crystallographica Section C: Structural Chemistry* **2015**, *71*, 3–8.
[52] A. Spek, *J. Appl. Crystallogr.* **2003**, *36*, 7–13.
[53] Deposition number 2328716 contains the supplementary crystallographic data for this paper. These data are provided free of charge by the joint Cambridge Crystallographic Data Centre and Fachinformationszentrum Karlsruhe Access Structures service.

Manuscript received: February 21, 2024
Accepted manuscript online: March 5, 2024
Version of record online: March 25, 2024